

Luminescence and damage thresholds of cerium-doped LaF₃ for ns-pulsed laser excitation at 248 nm

R. Lindner¹, M. Reichling¹, E. Matthias¹, H. Johansen²

¹Fachbereich Physik, Freie Universität Berlin, Arnimallee 14, 14195 Berlin, Germany
²Max-Planck-Institut für Mikrostrukturphysik, Weinberg 2, 06120 Halle, Germany

Received: 30 July 1998

Abstract. We have studied time-resolved luminescence spectra and laser damage thresholds of Ce:LaF₃ following excitation with 248 nm/14 ns laser pulses at room temperature for the two Ce concentrations 0.03 and 1 mol %. The relative intensities of the 5d-4f bands emitted from Ce³⁺ at regular and at perturbed lattice sites were found to vary linearly with time for the higher concentration and quadratically for the lower one. This can be explained by radiative energy transfer between the two sites and generation of new perturbed sites at a rate that only shows up for the low Ce concentration. Lifetimes of the respective emission bands were determined to be about 18 ns and 41 ns. Despite resonant absorption of the 5 eV photons, surprisingly high ablation thresholds – 16 J/cm² for 0.03% Ce, and 10 J/cm² for 1% Ce – were observed by the probe-beam deflection technique. The reason is the strong energy loss due to intense fluorescence and deposition of the nonradiative energy fraction in the bulk rather than at the surface. The depth of energy deposition was revealed by scanning electron microscopy in the form of distinctly different ablation morphologies for the two Ce concentrations.

PACS: 77.84.-s; 78.20.-e; 78.47.+p; 78.60.-b; 79.20.Ds

Cerium-doped LaF₃ exhibits a *strong fluorescence* around 4–4.5 eV composed of two bands originating from transitions between the lowest state of the 5d manifold to the 4f spin-orbit doublet of Ce³⁺ ions, with both states located in the band gap of LaF₃. This fluorescence is attributed to excited Ce ions at *regular lattice sites* and can be excited by optical and ionizing radiation [1, 2]. It has been extensively investigated to test the efficiency of the material as a high-density scintillator [1–6]. The emission depends on Ce concentration [1–3, 6], crystal temperature [1, 3–6], and excitation energy [1, 2]. Its decay constant varies somewhat with these parameters [1, 3, 4] and has for 5 eV excitation energy at room temperature a value of about 17 ns [1]. Even laser action has been observed within this wavelength range when pumped by ArF and KrF laser light [7].

On the low-energy side of the strong emission band a broad *weak fluorescence* appears, which is attributed to

Ce³⁺ ions at *lattice sites with a perturbed crystal field* [1–5]. The exact nature of the perturber has not yet been identified but is thought to be either an anion vacancy or interstitial, or substitutional oxygen [1, 2]. The reason that the weak fluorescence received considerable attention was that it degrades the scintillation efficiency of Ce-doped LaF₃. An energy transfer from Ce ions at regular lattice sites to those at irregular sites has been proposed [1, 2], the degree of which depends on Ce concentration and initial excitation energy. When exciting with photons in the energy range 5–6 eV, as done in [1, 3, 4, 6] and in our work, only the two fluorescence bands around 4–4.5 eV (strong emission) and 2.8–3.6 eV (weak emission) exist. The excitation scheme of both lattice sites with 248 nm is illustrated in Fig. 1. It is based on absorption probabilities given by Pedrini et al. [3] and energy shifts and splittings observed in our work, and will be discussed in Sect. 2.

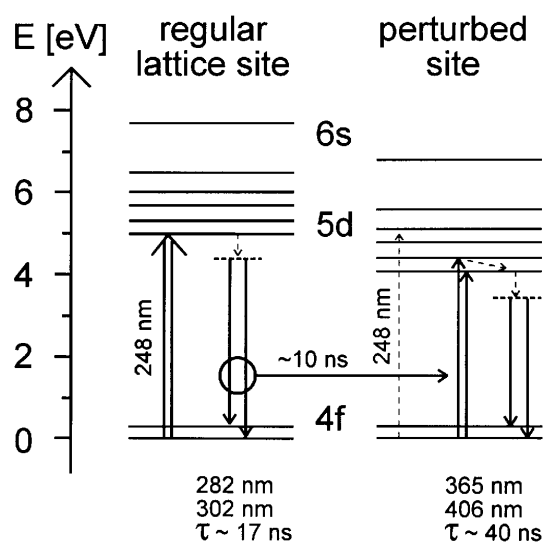


Fig. 1. Energy levels of Ce³⁺ ions at regular and perturbed lattice sites of LaF₃. The band gap of LaF₃ is 10.1 eV [12]; the ground state of the 4f doublet lies about 2.0 eV above the upper edge of the valence band [2, 13]. Energy spacings were constructed from absorption spectra in [3] and excitation as well as fluorescence energies in this work, as indicated

The fact that there is transfer of excitation energy from regular to perturbed Ce-ion sites was demonstrated by lifetime measurements for the strong and weak fluorescence bands. For 250 nm excitation the decay times of both bands were measured by Wojtowicz et al. [1] to be $\tau(286 \text{ nm}) = 16.7 \text{ ns}$ for undoped and $\tau(340 \text{ nm}) = 42.6 \text{ ns}$ for 5% Ce-doped LaF_3 . No significant variation with concentration was reported. The initial rise time of the 340 nm emission in doped samples unambiguously proves the population of excited 5d states at perturbed lattice sites within the decay time of the strong emission band. Up to now, the nature of this excitation transfer has not been well understood. Two mechanisms have been proposed [1–3]. One is reabsorption of the higher energy fluorescence, which presupposes the existence of Ce ions next to a lattice defect. The other is nonradiative energy conversion to Ce ions at perturbed sites. Transport by electron–hole pairs and excitons [6] can be excluded for the low excitation energy considered here, which only causes excitation of single 4f-electrons into the lowest state of the 5d manifold [3] (cf. Fig. 1). In this paper, we present comprehensive data on the change of spectral intensities with time, which prove radiative energy transfer from regular to perturbed Ce^{3+} sites but in addition provide evidence for conversion of regular into perturbed Ce sites by nonradiative transfer.

Let us now consider the laser resistivity of Ce:LaF₃. Any energy shift resulting from this excitation transfer between the two sites will heat the lattice. In principle, there are two sources of lattice heating. The important one is the Stokes shift between incident (5 eV) and reemitted (4.0–4.5 eV) radiation of the strong emission band. The other is the energy difference of 1 eV, on average, between the strong fluorescence from Ce^{3+} at regular lattice sites and reemission from Ce^{3+} at perturbed sites which, however, is much weaker and can be neglected. The first Stokes shift amounts to considerable lattice heating, which is likely to have detrimental consequences for the UV-laser resistivity of Ce:LaF₃. At the same time, this makes it an interesting case for studying the influence of controlled defects on laser damage of ionic crystals.

It has been suggested by several groups that laser damage of transparent crystals is caused by local defects, giving rise to populated states in the band gap which allow single photon absorption [8–10]. Such states could be of intrinsic nature, such as F- and H-centers and their aggregates, or extrinsic due to bulk impurities or structural defects. For example, it has been shown that the laser ablation threshold of nominally pure CaF_2 strongly depends on surface treatment [8, 11], whereas the content of bulk point defects seems to be of less importance. In general, the density of occupied states in the band gap is rather small and their energy position not very well defined. In this context, Ce:LaF₃ is an ideal model system since it has the 10.1 eV band gap of the LaF_3 [12] with the single 4f electron of Ce^{3+} occupying the energetically well defined $^2F_{5/2}$ ground state of the spin–orbit doublet, located about 2.0 eV above the valence band [2, 13]. Hence, 4f–5d excitations with 5 eV (248 nm) proceed within the band gap, much below the conduction band, and energy relaxation to the lattice can only take place via coupling of the Ce^{3+} impurity ions to the lattice.

An additional advantage is that the strong dipole-allowed 4f–5d absorption permits altering of the energy deposition depth by varying the Ce concentration and changing from

predominantly volume to near-surface heating. In this contribution we will correlate the damage morphology for two Ce concentrations, observed by scanning electron microscopy, with the energy deposition resulting from excitation and energy transfer from regular to perturbed lattice sites.

1 Experimental setup

We investigated two Ce:LaF₃ crystals with doping levels of 0.03 and 1 mol %, respectively, grown and polished by Optovac (North Brookfield, USA). Crystals were cut from raw material without any specific surface orientation. Unpolarized excimer laser light of 248 nm wavelength and 14 ns pulse length was focused onto the sample by a microscope objective of 25 mm focal length at perpendicular incidence. A circular aperture produced a spot at the surface with a toe hat intensity profile. For measurements of damage thresholds, the spot diameter was about 0.14 mm. The fluence was controlled by two rotatable dielectric mirrors and could be varied from 0.3 J/cm² to 40 J/cm². For fluorescence measurements we used much lower fluences of typically 26 mJ/cm² in order to avoid any kind of surface modification. Such low fluence levels were accomplished by moving the sample surface out of focus and increasing the laser spot size by about a factor of ten.

Fluorescence measurements were carried out with a gated optical multichannel analyser of 1 nm spectral resolution. The time resolution was 20 ns defined by the gate width. The gate position could be shifted from 35 ns to 130 ns after the excimer laser pulse. Fluorescence light was collected by a lens of 100 mm focal length, imaging the irradiated spot onto a fused silica fiberglass cable, which guided the light to the entrance slit of the optical multichannel analyzer. To improve the signal-to-noise ratio we accumulated spectra from the same surface spot for 500 laser shots.

For the determination of ablation thresholds we utilized the photoacoustic mirage technique described in detail elsewhere [14]. Briefly, a helium-neon laser probe beam passed the focus spot of the excimer laser parallel to the surface at a distance of 1.5 mm and was directed onto a narrow slit in front of a photomultiplier. Any heat or plasma expansion generating an acoustic wave that alters the refractive index of the air in front of the sample caused a transient deflection of the probe beam which, in turn, changed the intensity transmitted through the slit. As a function of incident laser fluence we measured both the deflection amplitude and the transit time, i.e., the time delay between the excimer laser pulse and the arrival of the acoustic wave at the probe beam position. Each data point was recorded from a spot at the surface which had not been irradiated by a preceding pulse.

In addition to quantitative ablation threshold measurements we inspected the surface morphology of damaged spots by scanning electron microscopy (SEM). Such images helped to identify the damage mechanism which we expected to be different for the two Ce concentrations because of the different optical penetration depths. Pedrini et al. [3] reported for a doping level of 0.05% Ce around 246 nm an absorption coefficient of 16.3 cm⁻¹, from which we estimate penetration depths of about 1 mm for the 0.03% and 30 μm for the 1% doped crystals, respectively. For 1% Ce the absorbed en-

ergy is deposited much closer to the surface compared to 0.03% concentration.

2 Fluorescence spectra

Fluorescence spectra for both Ce concentrations measured with various delay times are displayed in Fig. 2. The fluorescence intensity is given in arbitrary units, normalized to the excimer laser intensity and the number of applied laser shots. The main feature is the strong emission band of Ce^{3+} ions at *regular lattice sites* due to transitions between the lowest 5d state and the 4f spin-orbit doublet with the two maxima centered at 4.1 and 4.4 eV. It contains about 96% of the total intensity at 35 ns delay, decreasing with increasing time. The shape of the spectra is in accordance with the ones reported earlier for excitation energies around 5 eV [1, 3, 6, 7, 15, 16]. New is the time evolution of the fluorescence spectra which shows a rapid drop in intensity with increasing delay times while the spectral shape is preserved.

The Stokes-shifted emission from Ce^{3+} ions at *perturbed lattice sites* appears as a weak broad band centered about 1 eV below the main double peak. Magnified spectra of this weak emission are displayed in the insets of Figs. 2a and 2b for identical delay times as for the strong fluorescence. Due to inhomogeneous broadening probably originating from different perturber configurations [1, 3] the double peak structure of the 4f spin-orbit splitting is not well resolved, but can still be recognized. The weak fluorescence has different shapes for the

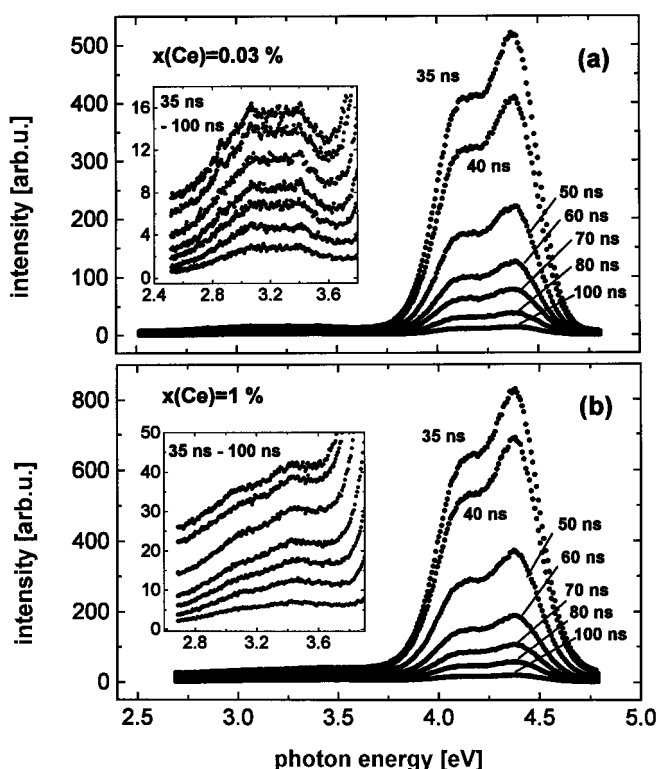


Fig. 2a,b. Fluorescence spectra of Ce:LaF₃ for the two Ce concentrations 0.03% (a) and 1% (b) and various delay times of the 20-ns gate. Each spectrum was recorded for 500 laser shots. The weak emission of Ce^{3+} ions on perturbed sites is magnified in the insets

two concentrations because for 1% Ce it is distorted by the low-energy tail of the strong emission band.

Since energy transfer between Ce^{3+} at regular and perturbed lattice sites has been proposed [1–3] it is of interest to extract from the spectra in Fig. 2 the time evolution of the intensities of both strong and weak emission bands. We did that by fitting Gaussians to the main peaks, and by ignoring the weak double peak structure of the low-energy fluorescence, approximating it by a single Gaussian. The procedure is illustrated by dotted lines in Figs. 3a and 3c for spectra taken at 100 ns delay with crystals of both concentrations. The two peaks in the strong emission band yield a 4f spin-orbit splitting of 0.28 ± 0.01 eV and a Stokes shift of 0.6 eV between the high-energy peak of the doublet and the 5 eV excitation energy. The spin-orbit splitting agrees well with values reported in the literature [1, 3, 6, 7, 16]. The two peaks located around 3.1 eV and 3.4 eV in the weak emission band also show a similar spin-orbit splitting for the two Ce concentrations. This again confirms that both strong and weak fluorescence bands originate from transitions between the lowest 5d state and the 4f doublet, differing only by the Stokes shift of the weak emission due to a disturbed crystalline environment.

Intensities obtained from such spectral fits at different delay times are plotted in Figs. 3b and 3d. Weighted exponential fits to the averaged data of both strong luminescence peaks yield decay times of 18 ± 1 ns for 0.03% and 17 ± 1 ns for 1% Ce, respectively, confirming the concentration independence reported in [1]. Decay times of the low-energy fluorescence are more than twice as long, amounting to 41 ± 1 ns and 40 ± 2 ns for the two concentrations. Again, these values are in good agreement with literature [1, 3, 7]. The decay curves show that the integrated intensity of the low-energy emission grows with time and eventually becomes even larger than the high-energy fluorescence. Note that the first two points of the low-energy emission around 40 ns in Figs. 3b and 3d do not fit the exponential decay pattern but indicate an initial increase of the low energy fluorescence with time. This behavior is particularly pronounced for 1% Ce and in agreement with observations reported in the literature [1]. It provided the basis for the proposed excitation transfer from regular to perturbed Ce^{3+} sites.

To investigate this energy transfer more quantitatively, we went one step further and compared at each individual delay the *relative intensities* of the weak and strong luminescence bands, normalized to the total fluorescence consisting of the sum of high- and low-energy emission. The result is shown in Fig. 4 for all measured delay times and both Ce concentrations. Open circles represent the decrease with time of the strong fluorescence from Ce^{3+} at regular lattice sites, solid dots indicate the corresponding growth of the weak emission intensity from perturbed Ce ions. Since the fluorescence intensity is proportional to the density of excited Ce^{3+} ions at the respective sites, the data in Fig. 4 directly reflect the population transfer of excited 5d states from regular to perturbed lattice sites.

From Fig. 4 we conclude that the 5 eV radiation *exclusively excites Ce ions at regular lattice sites*. Immediately after the pump pulse there is little or no population of 5d excited states at perturbed sites for either Ce concentration. Radiation emitted by 5d states of Ce^{3+} at regular sites is then reabsorbed by Ce^{3+} ground state ions at perturbed sites. Due

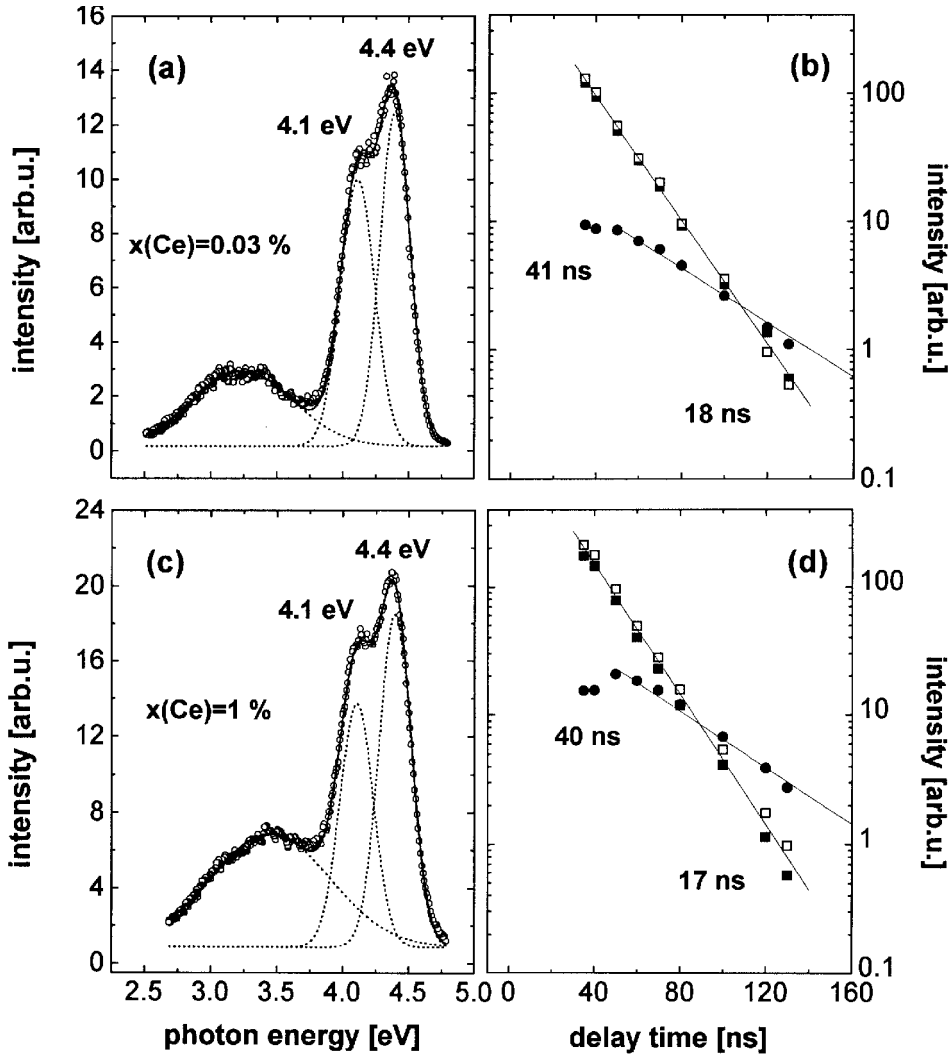


Fig. 3. a and c display fluorescence spectra of Ce:LaF₃ at 100 ns delay for 0.03% and 1% Ce, respectively. Dotted lines represent Gaussian fits to the data. Intensities of such fits for all measured delay times are plotted in b and d. Solid dots mark the decay of the low-energy fluorescence, open and solid squares the decay of the peaks around 4.1 eV and 4.4 eV, respectively. Straight lines are exponentials fitted to the data, resulting in the decay times indicated. The two points below 40 ns of the low-energy band were not included in the fit

to the much longer decay constant the density of excited Ce³⁺ at perturbed sites grows with ongoing time in proportion to the decline of excited Ce³⁺ at regular sites. Hence, we must

assume that there exists from the beginning a certain fraction of ground state Ce³⁺ ions at perturbed sites. The fact that these are not excited by the primary 5 eV radiation but

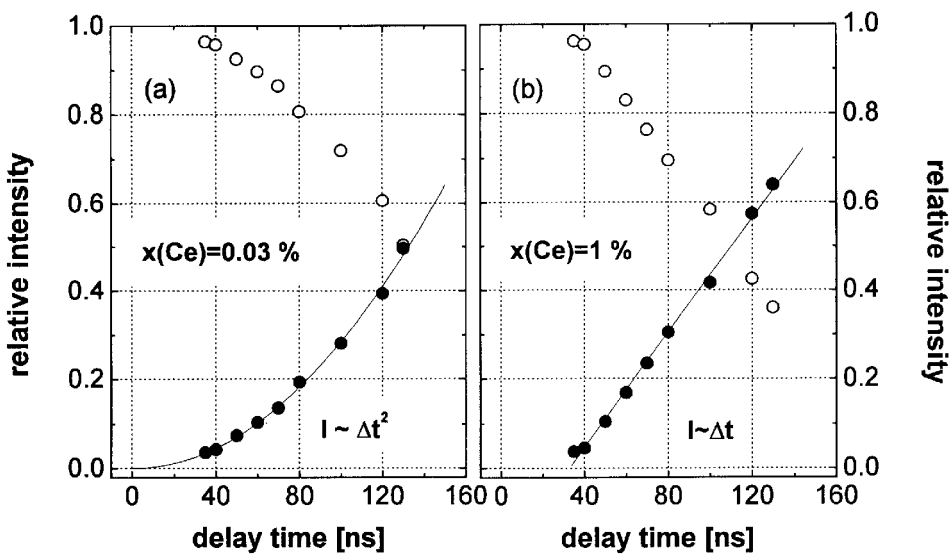


Fig. 4. Relative intensities of the low-energy (solid dots) and high-energy (open circles) fluorescence, normalized to the sum of both as a function of delay time. The intensity of the high-energy fluorescence consists of the sum of the 4.1 eV and 4.4 eV peak areas (compare Fig. 3). Solid lines indicate quadratic and linear growth of the 5d population at perturbed sites for low and high Ce concentrations, respectively

readily reabsorb the Stokes-shifted emission between 4.0 and 4.5 eV can be understood as a *resonance absorption effect*. As shown in Fig. 1 of [3], photons of 5 eV perfectly match the first absorption peak of Ce^{3+} at *regular* lattice sites for 0.05% Ce concentration. We adopt this result for our concentrations and propose that a similar absorption pattern, shifted by about 1 eV towards lower energies, applies to *perturbed* lattice sites, since absorption probabilities will, in first approximation, remain unaffected by an altered crystal field splitting. Then, 5 eV photons will not be absorbed. Instead, the strong fluorescence in the range 4.0–4.5 eV is reabsorbed by transitions to the two lowest states of the 5d manifold of Ce^{3+} at perturbed sites. This is the basis for Fig. 1.

We also notice in Fig. 4 that the overall *growth rate* of the Ce^{3+} 5d population at perturbed sites is roughly comparable for the two Ce concentrations. This is due to the fact that we plot relative intensities normalized to the sum of both low and high emission bands. The slightly faster growth rate for 1% Ce probably reflects a somewhat faster decay of the 5d states at regular lattice sites, although this is not apparent in the decay data shown in Figs. 3b and 3d.

A most surprising effect, however, is the apparent *quadratic* increase of the perturbed 5d population with time for 0.03% Ce, while for 1% Ce concentration the growth is only *linear*, as indicated by the solid lines in Figs. 4a and 4b, respectively. This observation suggests that there are actually two different processes taking place, *radiative energy transfer and creation of new perturbed sites*.

The linear and quadratic increase with time can be understood in the following way: If a fraction of the emitted higher energy fluorescence is reabsorbed by Ce ions at perturbed sites, the increase of the excited 5d state population $\Delta n_{5d}^p(t)$ with time is given by

$$\Delta n_{5d}^p \propto \sigma_{\text{abs}} n_{4f}^p(t) \phi(t) \Delta t.$$

Here, σ_{abs} is the cross section for reabsorption, $n_{4f}^p(t)$ the density of 4f ground states at perturbed sites, and $\phi(t)$ the photon flux originating from the decay of excited Ce ions at regular sites. Since we consider the change of relative intensities, the exponential decrease of the photon flux approximately cancels when dividing with the total fluorescence. From this equation it can be seen that a *linear increase* with time of the perturbed Ce^{3+} 5d population results when $n_{4f}^p(t) = \text{const}$. Such is the case when there is no significant change in Ce population at perturbed sites with time. It applies to the 1% Ce concentration for which a sizeable fraction of the Ce ions is already located at perturbed sites. This fraction responsible for reabsorption is sufficiently large so that any additional generation of perturbed sites will not significantly alter the reabsorption rate.

A *quadratic increase* with time of the relative intensity results when the Ce^{3+} population at perturbed sites grows with time, i.e., $n_{4f}^p(t) = \text{const} \Delta t$. This is observed at a doping level of 0.03% indicating that for very low concentrations the creation of new perturbed Ce^{3+} sites with ions in the 4f ground state plays a significant role. The probability for such process to happen is proportional to the elapsed time interval. The question arises about the nature of such process and the location of the new perturbed center. To answer this, we recall that anion vacancies or interstitials have been pro-

posed as perturbers [1, 2]. We also proposed in Fig. 1 that the Stokes shifted emission from 5d states at regular lattice sites exactly matches the 4f-5d energy gap for Ce at perturbed sites. Consequently, we conclude that – with a certain probability – the energy shift between primary excitation and reemission is consumed for pushing a neighbouring F^- out of its regular lattice site, thereby changing the crystal field and converting the originally unperturbed site of the 5d excited Ce ion into a perturbed one. After the Stokes-shifted emission, the 4f ground state remains in this perturbed site. Note that for energy reasons a similar conversion cannot take place at a perturbed site, apart from the negligible absorption of 5-eV photons. We also want to mention that the highest phonon frequencies of LaF_3 at room temperature are smaller by about two orders of magnitude and cannot easily accommodate a Stokes shift of 0.6–0.9 eV [17, 18].

3 Ablation thresholds

The total absorption of 248-nm light by Ce-doped LaF_3 within a comparatively small optical penetration depth should strongly affect the laser damage thresholds of these crystals. This expectation was based on the fact that the Stokes shifts between excitation and reemission deposit about 0.5–1.0 eV for each absorption event into the lattice. We decided to examine this conjecture by quantitative measurements of the damage onset with the probe-beam deflection technique [14]. Results for the two Ce concentrations are displayed in Fig. 5. In Figs. 5a and 5c the deflection amplitude is plotted against fluence of the incident excimer laser light for both concentrations. The steep rise of the deflection amplitude marks the threshold fluence for ablation. It amounts to 16 J/cm^2 for the crystal with 0.03% Ce and 10 J/cm^2 for the one with 1% doping.

The threshold fluences for the two concentrations in Figs. 5a and 5c only differ by a factor 1.6, despite the fact that the optical penetration depths deviate by a factor of 30. This points to a deeper energy deposition than suggested by the optical penetration depths taken from [3]. Self-induced transparency may contribute to such deeper penetration of the 248-nm radiation with the consequence that the deposited energy density is smaller and can be more easily accommodated by the lattice without damage.

The corresponding transit times of the acoustic waves between surface and probe beam, shown in Figs. 5b and 5d, confirm these threshold fluences by the onset of a decrease of transit time with increasing fluence, proving that shock waves accompany the material removal. In contrast, a normal sound wave driven by surface heating would result in a constant transit time [10]. We never recorded stronger sound waves despite the fact that cracks due to thermoelastic failure occur already much below the ablation threshold, as will be shown in Sect. 4. Probably, the sound of a single crack does not exceed the noise level of the apparatus.

Because of the strong absorption we expected significant surface heating followed by an acoustic wave with constant speed of sound. After all, the absorption reaches a maximum at 248 nm and – as discussed in Sect. 1 – the penetration depths are expected to be 1 mm and $30 \mu\text{m}$ for the 0.03% and 1% doped crystals, respectively. Instead, we only find evidence for faint surface heating below the ablation

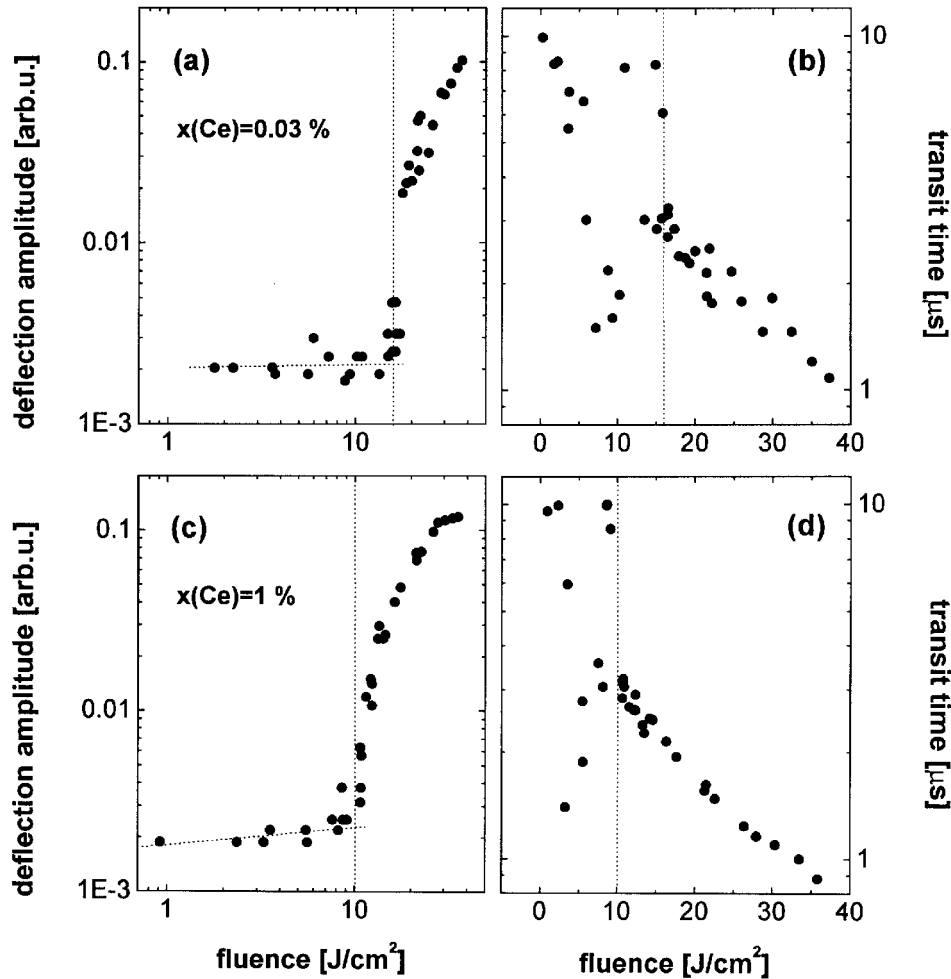


Fig. 5a–d. Deflection amplitudes (a), (c), and transit times (b), (d), as a function of applied fluence, measured with the probe-beam deflection technique [14] on Ce:LaF₃ crystals of 0.03% and 1% Ce concentration. Ablation threshold fluences and the development of the photoacoustic amplitude below threshold are marked by dotted lines

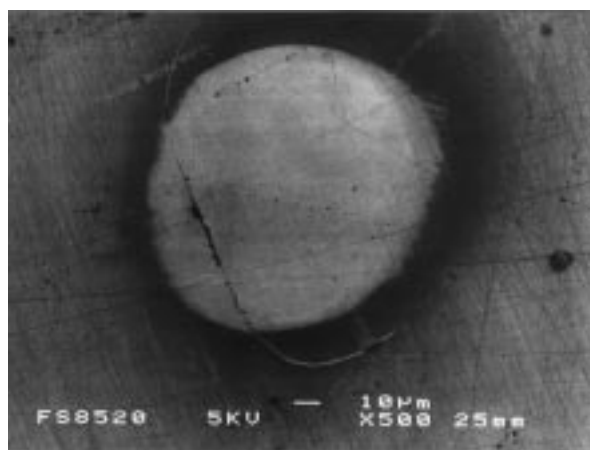
threshold in Fig. 5c in the form of a slight increase of deflection amplitudes in the range 1 to 10 J/cm² for 1% Ce concentration, and no effect at all for 0.03%. In accordance with the thresholds discussed above, this again implies that a large fraction of the absorbed energy is deposited in deeper parts of the crystal with the consequence that surface heating does not play an important role. The thermal diffusion length in the crystal, i.e., the distance heat can travel during the laser pulse, can be estimated to be 0.23 µm for a pulse length of 14 ns [19–21]. Therefore, most of the thermal energy is dissipated into the crystal and the surface exchanges hardly any heat with the air to produce a detectable acoustic wave. Since near-surface absorption is much stronger for the 1% doped crystal compared to the 0.03% one, there is a weak but significant increase in the acoustic deflection signal below the ablation threshold in Fig. 5c while for the low Ce concentration in Fig. 5a the acoustic signal intensity below threshold is not discernible from noise.

Another remarkable result is that the observed ablation thresholds for Ce:LaF₃ at our doping levels are comparable to those of polished CaF₂ [10]. This is greatly surprising in view of the fact that CaF₂ is highly transparent for 248-nm radiation whereas in Ce:LaF₃ the excimer laser light is totally absorbed. An explanation is furnished by the energy loss due to intense fluorescence of the Ce ions, which can easily be recognized by eye when the crystal is irradiated with UV

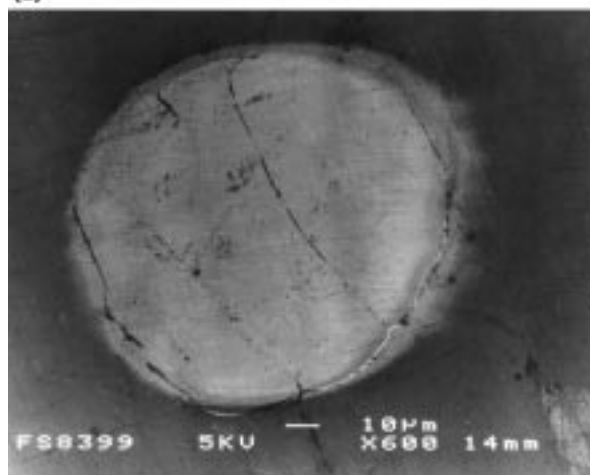
light. Apparently, the single 4f–5d electron excitation within the band gap does not couple strongly to the lattice, and the reemitted fluorescence carries away more than 70% of the initially absorbed energy. The rest is deposited as lattice heat with a minor fraction consumed for generating perturbed Ce sites.

4 Scanning electron microscopy

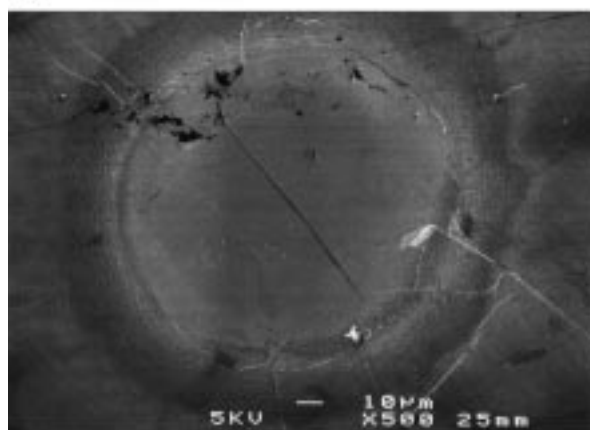
For a better understanding of the laser damage mechanism and thresholds for crystals with different Ce concentrations, we inspected a large number of irradiated spots with scanning electron microscopy (SEM). Three micrographs of typical damage patterns much below, around, and much above the ablation threshold are shown in Figs. 6a–c for the crystal with 0.03% Ce. Images of spots irradiated with fluences below or near ablation threshold are produced by changes in surface charging [22]. The general analysis of all irradiated spots at this sample reveals a major damage threshold around 15 J/cm² in good agreement with the probe beam deflection data in Fig. 5a. An illustration is given in Fig. 6b where at 16 J/cm² several major cracks can be observed. However, single cracks and surface modifications causing charging can already occur at fluences as low as 3 J/cm², as shown in Fig. 6a.



(a)



(b)



(c)

Fig. 6a–c. SEM images of surface spots on Ce:LaF₃ containing 0.03 mol % Ce impurities irradiated with 248 nm/14 ns laser pulses and fluences of 3.6 J/cm² (a), 16 J/cm² (b), and 37 J/cm² (c). The micrographs were recorded with 5 keV primary energy. The damage morphology is dominated by major cracks oriented along polishing scratches. Microcracks located at the rim of the spot in the region of maximum thermoelastic stress are visible in **b** and **c**. There is no indication of ablation even far above the threshold fluence of 16 J/cm²

In contrast to earlier observations on oriented CaF₂ surfaces [22, 23], crack damage in LaF₃ is not related to crystallographic directions but follows lines of surface damage, such

as polishing grooves, along which the fracture strength is reduced. In the extreme, this can lead to the formation of only one or two major cracks all the way through the irradiated spot, as can be seen in Fig. 6. At low fluences, for example, Fig. 6a shows a crack along a polishing groove inside the irradiated spot, which outside bends to follow another scratch. Major cracks as seen in Fig. 6 arise from thermoelastic stress in deeper parts of the crystal, consistent with the energy deposition depth discussed above.

At high fluence, much above damage threshold, Fig. 6c shows three types of thermoelastic stress relaxation. Major cracks originate at the spot periphery and propagate radially far beyond the laser beam diameter. The boundary of the irradiated spot is marked by a roughly circular crack. In addition, thermoelastic stress due to the temperature gradient occurs at the rim of the laser spot [22] leading to microfracture which can clearly be recognized at the spot periphery in Fig. 6c.

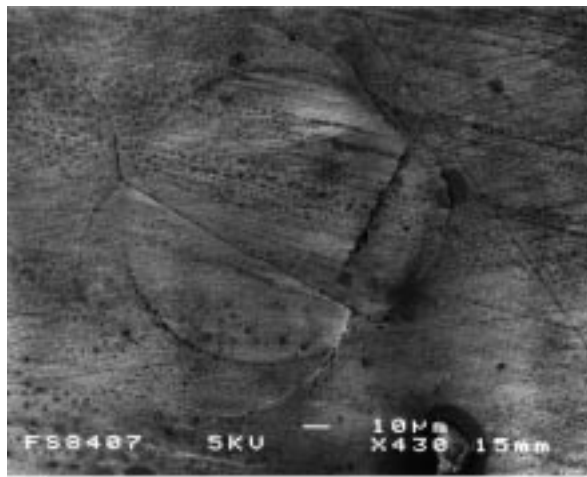
Notice, however, that there is no deeper ablation of the 0.03% doped crystal at any fluence, which again has to do with the energy deposition depth. Instead, it appears from the images shown in Fig. 6 that surface roughness is reduced with increasing laser fluence. Whereas for 3.6 J/cm² polishing scratches exhibit the same contrast inside and outside the irradiated region (Fig. 6a), those can barely be recognized around threshold at 16 J/cm² in Fig. 6b. At the highest fluence of 37 J/cm² polishing scratches disappeared completely and the inside of the spot is essentially characterized by an extremely smooth surface topography (see Fig. 6c), apart from the one deep crack across the spot. We attribute this smoothing to both ablation, as proved by Fig. 5a, and strong volume heating up to the limit of plasticity.

For the 1% doped crystal we also observe surface modifications at fluences much below the ablation threshold. The first surface alteration appeared as charging in the SEM images around 0.9 J/cm² and the first crack damage was found around 3.5 J/cm². In comparison, these thresholds are comparable to those for the 0.03 mol % doped crystal. Again, crack damage follows polishing grooves as shown in the example in Fig. 7a for 5.5 J/cm². This means heating begins far below the ablation threshold in a near-surface region defined by the shallow optical penetration depth of about 30 µm.

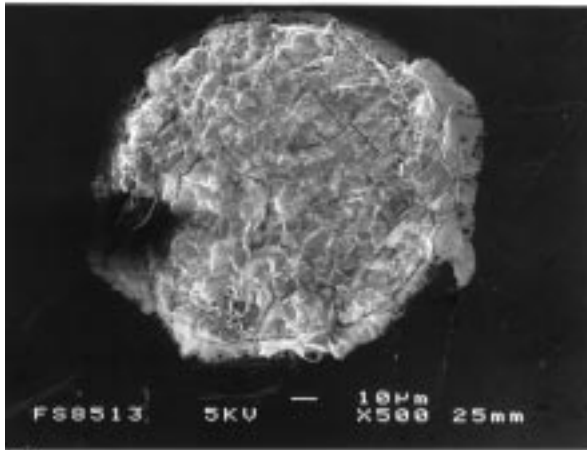
At higher fluences the energy deposition near the surface of the 1% doped crystal leads to completely different damage morphologies as compared to those observed for 0.03% concentration in Fig. 6. Images in Figs. 7b and 7c represent irradiations with fluences well above the ablation threshold where we find massive material removal from the entire irradiated area. At 14 J/cm² in Fig. 7b fracture and fragment removal is the dominant feature with no sign of melting. A circular crack around the periphery can be made out, quite similar to the one observed in Fig. 6b, but the high density of microcracks in the rim of the irradiated spot is no longer present. For still higher fluences melting and ejection of molten material in radial directions as illustrated for 36 J/cm² in Fig. 7c.

5 Summary and conclusion

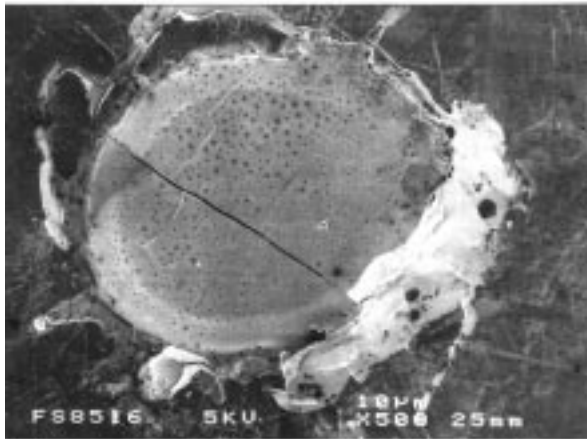
The interaction of 248 nm/14 ns pulses with Ce:LaF₃ was studied for doping concentrations of 0.03% and 1%. Three types of investigations were carried out. First, the lumi-



(a)



(b)



(c)

Fig. 7a–c. SEM images of surface spots on Ce:LaF₃ containing 1 mol % Ce impurities irradiated with 248 nm/14 ns laser pulses and fluences of 5.5 J/cm² (a), 14 J/cm² (b), and 36 J/cm² (c). The images were obtained with 5 keV primary energy. **b** and **c** illustrate the damage morphology, which is dominated by material removal and surface melting

nescence intensity emitted from Ce³⁺ 5d states was measured as a function of delay time with regard to the excitation pulse. Second, utilizing the probe beam deflection technique, ablation thresholds were determined for crystals with these two Ce concentrations. Finally, scanning

electron microscopy was applied to inspect the damage morphology for laser fluences below and above the ablation threshold.

Luminescence spectra consist of strong emission from Ce³⁺ 5d states at regular and weak emission from 5d states at perturbed lattice sites. The time evolution of the relative intensities in the strong and weak luminescence bands shows a linear increase of the relative intensity from 5d states at perturbed sites for 1% Ce concentration and a quadratic increase in the case of 0.03% Ce. The linear increase supports the general concept of radiative energy transfer from excited Ce ions at regular lattice sites to ions at perturbed sites. The quadratic increase of the relative intensity from perturbed sites at low Ce concentration provides evidence for non-radiative conversion of excited Ce³⁺ from regular into perturbed lattice sites. We suggest that the mechanism for such conversion is a Stokes-shift-driven move of an adjacent anion into a defect position, resulting in a crystal field distortion.

Since most of the absorbed energy is reemitted by 5d-4f transitions proceeding within the band gap of LaF₃, the Ce:LaF₃ crystal is an interesting test case for laser damage. The residual energy deposition into the lattice is mainly by a Stokes shift of about 0.5–1.0 eV for the excitation of Ce³⁺ at regular lattice sites. We find ablation thresholds of 16 J/cm² for crystals with 0.03% Ce and 10 J/cm² for those with 1% Ce. The fact that these fluences are quite comparable to the ablation threshold of polished CaF₂ emphasizes the heavy energy loss by luminescence. In addition, the strong absorption of 248-nm light leads to small optical penetration depths of about 1 mm and 30 µm for low and high Ce concentration, which is at least two orders of magnitude larger than the thermal diffusion length for a pulse duration of 14 ns. For this reason we find no evidence of surface heating below the ablation threshold for the crystal with 0.03% Ce and only small heating for the one with 1% Ce.

SEM images of all irradiated spots complete the picture about surface modifications and damage as a function of fluence. The crystal response is governed by bulk heating and crack damage when thermoelastic stress exceeds a critical value. Crack damage thresholds were found to be around 3 J/cm² for crystals with either concentration. An ablation threshold of 16 J/cm² was measured by probe-beam deflection in the case of low Ce concentration. For the 1% Ce concentration the damage threshold found by SEM imaging is about 3 times lower than the ablation threshold of 10 J/cm², observed by probe-beam deflection. The lower threshold for the crystal with higher Ce concentration is attributed to the stronger near-surface absorption. This interpretation is supported by the observed strong differences in damage and ablation topography for both crystals. For low Ce concentration, i.e., predominant volume heating, crack damage is the main result found even for spots irradiated with fluences above the ablation threshold. This means that thermoelastic stress is released by crack formation and, at very high fluences, even plastic motion. In the case of the 1% Ce crystal, for which the energy density is deposited closer to the surface, fluences above the ablation threshold cause strong disintegration by ablation and melting in the high fluence regime.

Acknowledgements. This work was supported by the Deutsche Forschungsgemeinschaft, Sfb 337.

References

1. A. J Wojtowicz, M. Balcerzyk, E. Berman, A. Lempicki: Phys. Rev. B **49**, 14880 (1994)
2. W.W. Moses, S.E. Derenzo, M.J. Weber, A.K. Ray-Chaudhuri, F. Cerina: J. Lumin. **59**, 89 (1994)
3. C. Pedrini, B. Moine, J.C. Gacon, B. Jacquier: J. Phys. Cond. Mater. **4**, 5461 (1992)
4. P. Rodnyi, E. Melchakov, N. Zakharov, I. Munro, A. Hopkirk: J. Lumin. **65**, 85 (1995)
5. E.D. Thoma, H. Shields, Y. Zhang, B.C. McCollum, R.T. Williams: J. Lumin. **71**, 93 (1997)
6. L.R. Elias, Wm.S. Heaps, W.M. Yen: Phys. Rev. B **8**, 4989 (1973)
7. D.J. Ehrlich, P.F. Moulton, R.M. Osgood, Jr.: Opt. Lett. **5**, 339 (1980)
8. K. Tanimura, N. Itoh: Nucl. Instrum. Methods B **46**, 207 (1990)
9. J.T. Dickinson: Nucl. Instrum. Methods B **91**, 634 (1994)
10. S. Gogoll, E. Stenzel, M. Reichling, H. Johansen, E. Matthias: Appl. Surf. Sci. **96-98**, 332 (1996)
11. E. Stenzel, S. Gogoll, J. Sils, M. Huisinga, H. Johansen, G. Kästner, M. Reichling, E. Matthias: Appl. Surf. Sci. **109/110**, 162 (1997)
12. C.G. Olson, M. Piacentini, D.W. Lynch: Phys. Rev. B **18**, 5740 (1978)
13. H. Merenga, J. Andriessen, C.W.E. Van Eijk: Radiat. Meas. **24**, 343 (1995)
14. E. Matthias, J. Siegel, S. Petzoldt, M. Reichling, H. Shurk, O. Käding, E. Neske: Thin Solid Films **254**, 139 (1995)
15. Wm.S. Heaps, L.R. Elias, W.M. Yen: Phys. Rev. B **13**, 94 (1976)
16. K.H. Yang, J.A. DeLuca: Appl. Phys. Lett. **31**, 594 (1977)
17. E. Liarokapis, E. Anastassakis, G.A. Kourouklis: Phys. Rev. B **32**, 8346 (1985)
18. F. Cerdeira, V. Lemos, R.S. Katiyar: Phys. Rev. B **19**, 5413 (1979)
19. L.A. Remizova: High Temperature **16**, 661 (1978)
20. Landolt-Börnstein NS III 7 a 23
21. W.G. Lyon, D.W. Osborne, H.E. Flotow, F. Grandjean, W.N. Hubbard, G.K. Johnson: J. Chem. Phys. **69**, 167 (1978)
22. S. Gogoll, E. Stenzel, H. Johansen, M. Reichling, E. Matthias: Nucl. Instrum. Methods B **116**, 279 (1996)
23. M. Reichling, H. Johansen, S. Gogoll, E. Stenzel, E. Matthias: Nucl. Instrum. Methods B **91**, 628 (1994)